Nuclear Instruments and Methods in Physics Research A 699 (2013) 230–234

Contents lists available at SciVerse ScienceDirect

Nuclear Instruments and Methods in Physics Research A

journal homepage: www.elsevier.com/locate/nima

Development of high performance Avalanche Photodiodes and dedicated analog systems for HXI/SGD detectors onboard the Astro-H mission

T. Saito [a,*], T. Nakamori [a], M. Yoshino [a], H. Mizoma [a], J. Kataoka [a], K. Kawakami [b], Y. Yatsu [b], M. Ohno [c], K. Goto [c], Y. Hanabata [c], H. Takahashi [c], Y. Fukazawa [c], M. Sasano [d], S. Torii [d], H. Uchiyama [d], K. Nakazawa [d], K. Makishima [d], S. Watanabe [e], M. Kokubun [e], T. Takahashi [e], K. Mori [e], H. Tajima [f]

[a] Research Institute for Science and Engineering, Waseda University, 3-4-1 Ohkubo, Shinjuku, Tokyo, Japan
[b] Tokyo Institute of Technology, 2-12-1 Ookayama, Meguro, Tokyo 152-8551, Japan
[c] Department of Physical Science, Hiroshima University, 1-3-1 Kagamiyama, Higashi-Hiroshima, Hiroshima, Japan
[d] Department of Physics, University of Tokyo, 1-3-1 Hongo, Bunkyo, Japan
[e] Institute of Space and Astronautical Science, Japan Aerospace Exploration Agency (ISAS/JAXA), 3-1-1 Yoshinodai, Sagamihara, Kanagawa, Japan
[f] Solar-Terrestrial Environment Laboratory, Nagoya University, 461-8601 Furo, Chikusa, Nagoya, Aichi, Japan

Astro-H HXI/SGD Team

ARTICLE INFO

Available online 26 May 2012

Keywords:
Avalanche Photodiode
Gamma-rays
Scintillation detection

ABSTRACT

Hard X-ray Imager and Soft Gamma-ray Detector are being developed as onboard instruments for the Astro-H mission, which is scheduled for launch in 2014. In both detectors, BGO scintillators play key roles in achieving high sensitivity in low Earth orbit (LEO), by generating active veto signals to reject cosmic-ray events and gamma-ray backgrounds from radio-activated detector materials. In order to maximize background rejection power, it is also important to minimize the energy threshold of this shield. As a readout sensor of weak scintillation light from a number of BGO crystals in a complicated detector system, high performance, reverse-type Avalanche Photodiodes (APDs), with an effective area of 10×10 mm^2 are being employed, instead of bulky photomultiplier tubes (PMTs).Another advantage of using APDs is their low power consumption, although the relatively low gain of APDs (compared to conventional PMTs) requires dedicated analog circuits for noise suppression. In this paper, we report on the development and performance of APD detectors specifically designed for the Astro-H mission. In addition to APD performance, various environmental tests, including radiation hardness and qualification thermal cycling, will be described in detail. Moreover, a dedicated charge sensitive amplifier and analog filters are newly developed and tested here to optimize the performance of APDs to activate fast veto signals within a few μs from the BGO trigger. We will also report on overall performance testing of a prototype BGO detector system that mimics the data acquisition system onboard Astro-H.

1. Introduction

Astro-H represents the sixth satellite of the Japanese X-ray observatory series [1], and is scheduled for launch in 2014 aboard the H-II A rocket. This mission covers a very wide energy range from 0.3 to 600 keV with four instruments. Two of the onboard instruments, Hard X-ray Imager (HXI [2]) and Soft Gamma-ray Detector (SGD [3]), employ $Bi_4Ge_3O_{12}$ (BGO) active shields that enclose the main detectors to achieve unprecedented high sensitivity in low Earth orbit (LEO). Using the anti-coincidence technique, the BGO active shields effectively reject background events such as cosmic-ray particles, radiation from the activated shield itself, and photons beyond the field of view. Hard X-ray Detector (HXD) onboard the Suzaku satellite [4,5] has demonstrated in orbit that the BGO active shields work properly and achieve high sensitivity for 10–600 keV. In order to read out weak scintillation light from a number of BGO crystals in a complicated detector system, Avalanche Photodiodes (APDs) are employed in the Astro-H mission instead of bulky photomultiplier tubes (PMTs) used aboard Suzaku. APD is a compact semiconductor photosensor equipped with an internal signal amplifying function realized by a strong gradient of an electric field in a depletion layer [6,7]. A reverse-type APD is ideally suited for detecting scintillation photons [8–10], where its thin multiplying region is located at the surface. Photons from a scintillator are sufficiently absorbed within the first few μm of the depletion layer and generate

* Corresponding author.
E-mail address: songbird@fuji.waseda.jp (T. Saito).

0168-9002/$ - see front matter © 2012 Elsevier B.V. All rights reserved.
http://dx.doi.org/10.1016/j.nima.2012.05.061

electrons undergoing full multiplication. In-orbit operation has been successfully established by the Tokyo Tech pico-satellite Cute-1.7+APD II over several years, monitoring the global distribution of low energy particles trapped in LEO [11,12]. However, a relatively low gain compared to that of conventional PMTs and large capacitance conversely require dedicated analog circuits for noise suppression, in order to achieve as low an energy threshold as possible. Ohno et al. [13] described an overview of the BGO readout system, and this paper focuses on the performance of the APD sensor and subsequent analog systems (Fig. 1).

2. Development of Avalanche Photodiodes

Fig. 2 shows the reverse-type APD that we developed as the Flight Model (FM-APD). This model is based on the S8664 series [7–9] manufactured by Hamamatsu with an active area of $10 \times 10\,mm^2$. We arranged the positions of both anode and cathode pins to prevent discharge and for easier soldering. We also replaced the window material conventionally made of epoxy resin with silicone resin from the standpoint of thermal cycle tolerance described in the following subsection. When integrated as a completed system, the FM-APD is mounted as a BGO active shield detector in an electromagnetic shield made of aluminum, 200-μm-thick. This is because the APDs, being characterized by low gains, are sensitive to noise generated by external electromagnetic fields.

2.1. Thermal test

All onboard instruments will experience a severe thermal environment just after launch. In order to maintain designed performance during a mission, the APD assembly must not be delaminated through the launch. We had two alternative APD models with different window materials. One model uses epoxy resin as has been conventionally used. The other model uses silicone resin as well as photodiodes applied for the Fermi-LAT calorimeter [14,15], since micro cracks appeared in the epoxy window during strict thermal cycling. Although the thermal conditions we expect during the launch of Astro-H are not as serious as in the case of Fermi, we conducted a thermal cycle tolerance test for the APDs adhered to BGO crystals. We fabricated samples consisting of a block of BGO ($4 \times 3 \times 0.5\,cm^3$) for coupling to the APDs with epoxy and silicone windows using a space-grade silicone adhesive (DC93-500; Dow Corning). In considering the thermal conditions expected during the launch, we defined a 10-h cycle between 45 °C and −35 °C with a gradient of 20 °C/h dwelling at both the top and bottom temperatures for an hour. We then irradiated a ^{137}Cs source on these samples and traced pulse heights corresponding to 662 keV before and after several cycles. Fig. 3 shows the result, revealing a significant difference between the epoxy and silicone windows. Thus, the optical performance of an APD with an epoxy window deteriorates more quickly than that of one with a silicone window. Therefore, we decided to adopt silicone window APDs for the Flight Model of Astro-H.

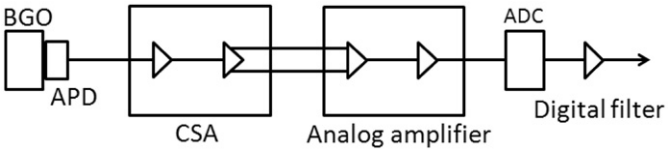

Fig. 1. Flowchart of signal processing by the BGO readout system. Also see Ohno et al. [13].

2.2. Radiation tolerance test

A decrease in breakdown voltage and an increase in dark currents should pose major concerns about possible damage caused by radiation during an entire mission. We verified the tolerance to ^{60}Co irradiation with a dose of 10 krad, which we assume is a conservative estimate for a mission lasting more than ten years. We also measured the differences in breakdown voltage before and after irradiation in 57 APDs, as shown in Fig. 4. This histogram indicates no substantial change in breakdown voltage, as the differences were 0.4 V at most. Table 1 summarizes the noise characteristics. In this work, we assumed −15 °C as

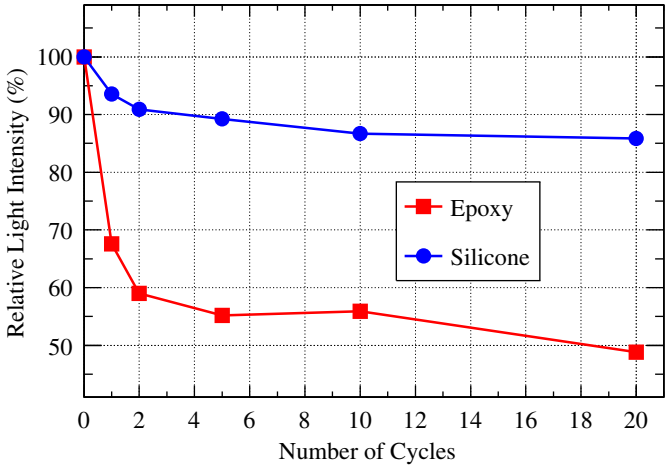

Fig. 3. Relation between relative light intensity normalized at the starting point and the number of cycles. Light intensity is calculated from a gamma-ray pulse height of 662 keV (^{137}Cs).

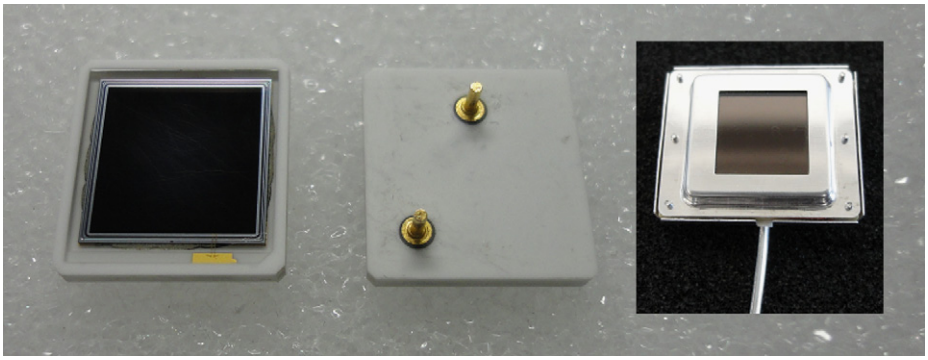

Fig. 2. Photo of the Flight Model APD.

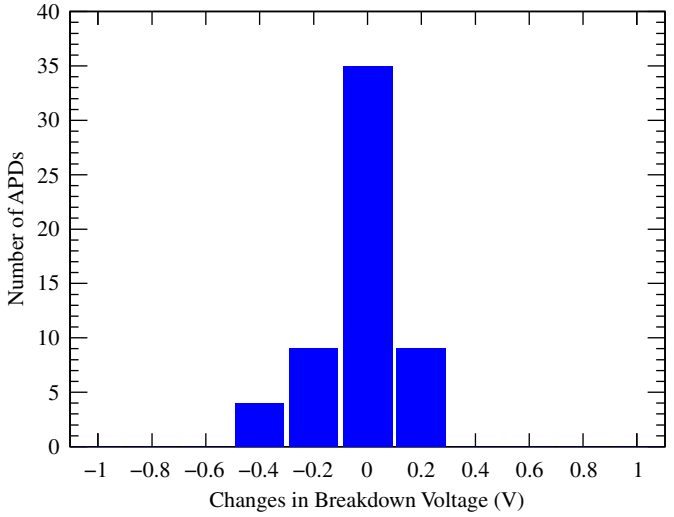

Fig. 4. Histogram showing changes in breakdown voltage before and after ^{60}Co irradiation.

Table 1
APD performance at −15 °C before and after irradiation.

Total dose (krad)	APD dark current (nA)	Testpulse width (keV)
0	0.3	10.6
10	1.9	13.2

the in-orbit temperature. We coupled a reference BGO ($1\times1\times1$ cm^3) to the APD and obtained the energy spectrum of a ^{137}Cs source and simultaneously an external test pulse at −15 °C, where deviation of the test pulse spectrum indicates the noise level of this system. Although the dark current increased six times after irradiation, the widths (FWHM) of the test pulse spectrum only increased 3 keV, suggesting that our APD has sufficient radiation tolerance that would not adversely affect its performance as a scintillation detector. Strictly speaking, however, this is too optimistic because the APD suffers bulk damage mainly caused by high energy protons as well as surface damage demonstrated by ^{60}Co irradiation. In fact, Kataoka et al. [16] reported that significant increase in bulk current, which is the multiplied component of the APD dark current. Assuming that about 5 percent of the total dose will be attribute to high energy protons, they concluded that the energy threshold of the BGO readout for Astro-H may increase by a factor of 1.3–1.6 after the expected five-year life of the Astro-H mission, whereby its impact on background rejection power must be carefully considered before the launch.

2.3. Pre-Flight Model APD acceptance test

Since more than 130 APDs will be fabricated for use onboard Astro-H, we must establish how to screen FM-APDs after mass production. The dark current is composed of surface current and bulk current (with only the latter being multiplied in proportion to the avalanche gain) [16]. At the in-orbit temperature the bulk current should be dominant, while at room temperature it is not clear which component is responsible for the net dark current. An APD with relatively higher bulk current is likely to show higher dark current even at low temperatures. This is why an important selection criterion is the amount of dark current at the in-orbit temperature, where we have defined an upper limit of 0.4 nA with operating voltage corresponding to an avalanche gain of 50. Since the manufacturer (Hamamatsu) provides us with qualification sheets for all APDs including dark current and recommended operating voltage at 25 °C, we determined an appropriate upper limit to this value of dark current. Nevertheless some APDs remain with high dark currents over the limit of 0.4 nA at −15 °C. A few APDs also have anomalous characteristics of dark current along with temperature changes, but satisfy the upper-limit condition around the in-orbit temperature. We should exclude these strange samples through the acceptance test. We therefore evaluated 20 pre-Flight Model (preFM) APDs having the same structures as the FM-APD candidates at three temperatures around −15 °C. In fact, one preFM-APD (preFM16) exceeded the limit and another (preFM4) showed different variations in dark current, along with temperature as shown in Fig. 5. Moreover, only preFM4 showed different operating voltage changes along with temperature changes as shown in Fig. 6. In order to screen out these noisy APDs even at the in-orbit temperature, we decided to measure the dark current characteristics at three points around the in-orbit temperature.

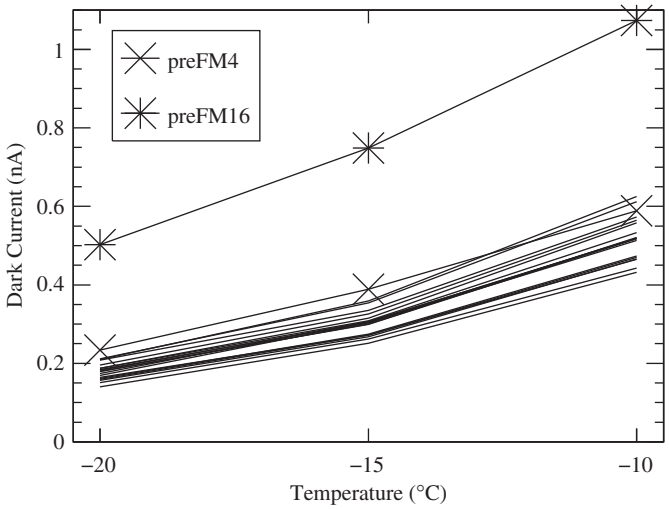

Fig. 5. Dark currents of the 20 preFM-APDs at −20 °C, −15 °C and −10 °C with a gain of 50. One (preFM16; asterisk) exceeded the upper limit of 0.4 nA. Another (preFM4; X marker) satisfied the limit with a strange temperature characteristic.

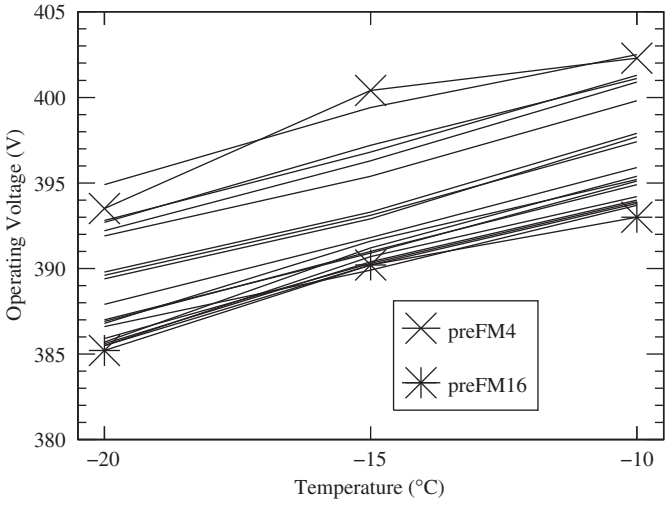

Fig. 6. Operating voltages of 20 preFM-APDs at −20 °C, −15 °C and −10 °C at a APD gain of 50. Only preFM4 showed different operating voltage changes, as well as dark current (see Fig. 5), along with temperature changes. The others including preFM16 showed common behavior.

Based on the results of the preFM trial, we expect 90 percent of FM-APDs to pass this test.

3. Development of analog systems

The relatively low gain of APDs (compared to conventional PMTs) and the APD capacitance ($\sim$270 pF) require analog systems specialized in terms of noise performance. We thus developed a charge sensitive amplifier (CSA) and an analog amplifier to achieve a better *S*/*N* ratio of analog signals.

3.1. Charge sensitive amplifier

Since the APD has relatively large capacitance as a photodetector, the capacitive noise is dominant at the in-orbit temperature [16]. There, we developed a dedicated CSA specialized in noise performance for a detector with large capacitance. Using our CSA, we obtained the pulse height spectra of a test pulse with various capacitors, where shaping with a time constant of 2 μs was made in the main amplifier. And then from deviations of the test pulse spectra, we extracted the equivalent noise charges (ENC) as a function of capacitance. We also obtained the pulse height of a Si photodiode using 59.5 keV gamma-rays from a ^{241}Am source, in order to normalize the obtained ENC into a unit of energy. Fig. 7 shows the obtained capacitance gradient well fitted with a slope of 9.8 pF/eV, as compared with a commercially available CSA (Clear Pulse 580S1). And as we estimated that the FM-APD has $\sim$400 pF including readout cables, the ENC (FWHM) should be 6 keV with a small dependence on capacitance. Thanks to a better capacitance gradient (i.e., less affected by detector capacitance) than that of commercial CSAs, our CSA offers high readout performance, even when using a detector with relatively high capacitance like the developed APD described in this paper.

3.2. Analog amplifier for the Astro-H mission

Both the CSA and an analog main amplifier play important roles in achieving a good *S*/*N* ratio. Due to limited space in the spacecraft as well as low power consumption, the main amplifier is specifically designed to be as simple as possible, namely, a single-stage differential and integrating circuit. We performed optimization in the time constants of integration under a constraint on peaking time shorter than the 5 μs necessary to generate an effective veto signal to the main detector as quickly as possible. We also obtained the energy spectra of a ^{137}Cs source and a reference test pulse at -15 °C with various time constant-τ. Then, we evaluated each deviation (FWHM) of the test pulse spectrum that we defined here as an energy threshold. Fig. 8 shows the result, where $\tau = 1.1$ μs achieved the best *S*/*N* ratio. Note that in order to keep the peaking time constraint, we had to add another differential filter (<50 μs) in cases with $\tau > 1.3$ μs that caused a worse *S*/*N* ratio. This was probably because the signals are mainly composed of low frequency [13] suppressed by this additional high pass filter. Here, we applied τ of 1.0, 1.1, and 1.2 μs for further studies.

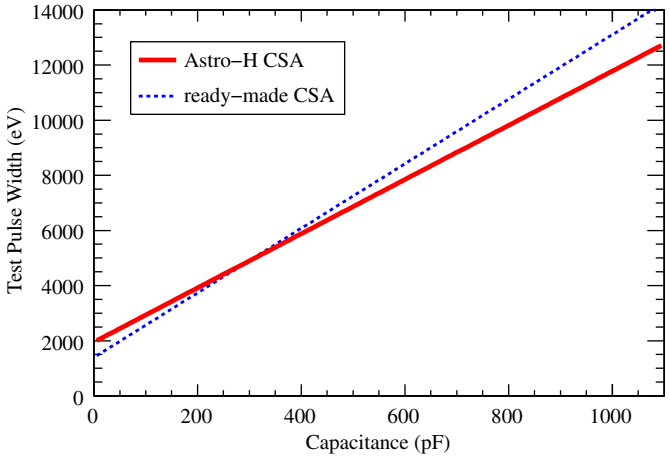

Fig. 7. Comparison of test pulse width relative to input capacitance. The solid and dashed lines represent the CSA developed in this work and a commercial one, respectively.

3.3. Integrated system performance

Finally, the signal is sampled by an ADC and processed by a digital filter equipped on an FPGA to maximize the *S*/*N* ratio [17]. The digital filter that works as a band-pass filter consists of 16 delay units with 8-bit precision coefficients. Ohno et al. [13] described the design of the digital filter. We integrated the entire readout system for a single BGO shield measuring $8 \times 8 \times 4$ cm^3

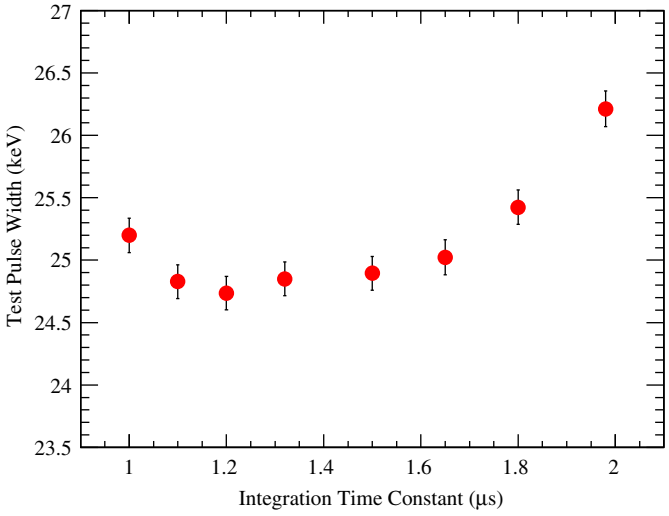

Fig. 8. Comparison of energy threshold along with integrating time constants.

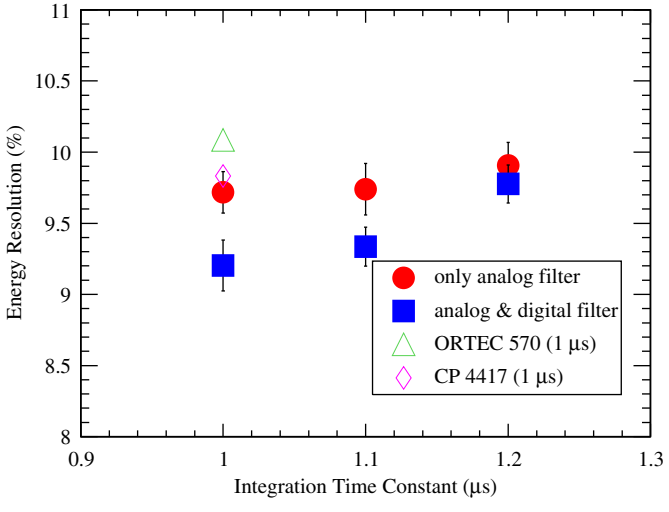

Fig. 9. Comparison of FWHM energy resolutions for 662 keV with various integration time constants. Filled circles and squares indicate the analog filter of this work without and with the digital filter, respectively. Triangular and diamond-shaped markers represent commercial shaping amplifiers for reference.

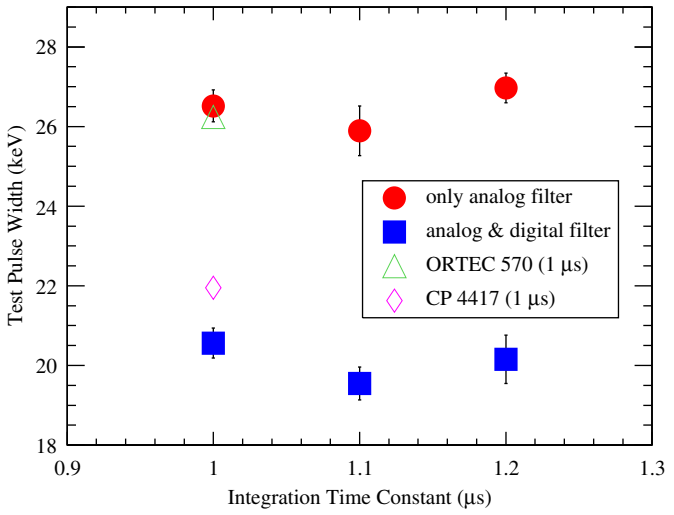

Fig. 10. Comparison of noise level with various integration time constants. The markers are identical to those shown in Fig. 9.

with a preliminary data acquisition system to be loaded on the spacecraft. We irradiated a ^{137}Cs source and first evaluated the energy resolution for 662 keV gamma-rays. Fig. 9 compares the energy resolutions along with τ, where the digital filter effectively improves performance in every case. A shorter τ is apparently preferable for better resolution. This figure also shows that combining the analog systems and digital filter achieved excellent performance compared to commercial shaping amplifiers, such as the Models 570 (ORTEC) and CP 4417 (ClearPulse). We also evaluated the noise level by using a test pulse spectrum, as well as conducting the above experiments, the results of which are shown in Fig. 10. The benefit of the digital filter is also apparent and $\tau = 1.1$ μs provides the best noise performance.

4. Summary

Hard X-ray Imager (HXI) and Soft Gamma-ray Detector (SGD) onboard the Astro-H satellite employ BGO active shields using the APDs as photosensors. Since the APDs are exposed to a severe environment just after launch, we evaluated the APDs by thermal cycle and by conducting a radiation tolerance test. We decided to apply silicone resin as the APD window material as the optical performance of epoxy resin deteriorates quickly during thermal cycles. We verified the sufficient radiation tolerance by ^{60}Co irradiation with a dose of 10 krad, since the breakdown voltage of the APDs and the S/N ratio did not vary significantly at the in-orbit temperature. Moreover, we established a method of conducting the Flight Model (FM) APD screening test using 20 pre-Flight Model APDs, where we measure the dark current and operating voltages around the in-orbit temperature at three points. The absolute value, behaviors, and temperature will be used as the screening criteria. In order to achieve as low an energy threshold as possible, we developed a specific CSA and analog amplifier. The developed CSA proved to have a gradual capacitance slope, thereby achieving high performance when used with a large capacitance detector such as APDs. Under the constraint on peaking time shorter than 5 μs, we optimized the time constants of our analog amplifier to achieve the lowest noise level possible. As a result, our analog amplifier showed the best performance at integrating time constants of 1.1 or 1.2 μs. Finally, in combination with the digital filter of our mission, the noise performance of our analog amplifier proved to be better than commercially available analog shapers.

Acknowledgment

We deeply appreciate the insightful comments and suggestions of the referee to improve this manuscript.

References

[1] T. Takahashi, et al., Proceedings of SPIE 7732 (2010) 27.
[2] M. Kokubun, et al., Proceedings of SPIE 7732 (2010) 33.
[3] H. Tajima, et al., Proceedings of SPIE 7732 (2010) 34.
[4] T. Takahashi, et al., Publications of the Astronomical Society of Japan 59 (2007) 35.
[5] M. Kokubun, et al., Publications of the Astronomical Society of Japan 59 (2007) 53.
[6] J.P. Pansart, Nuclear Instruments and Methods in Physics Research Section A 387 (1997) 186.
[7] J. Kataoka, T. Saito, Y. Kuramoto, T. Ikagawa, Y. Yatsu, J. Kotoku, M. Arimoto, N. Kawai, Y. Ishikawa, N. Kawabata, Nuclear Instruments and Methods in Physics Research Section A 541 (2005) 398.
[8] T. Ikagawa, J. Kataoka, Y. Yatsu, N. Kawai, K. Mori, T. Kamae, H. Tajima, T. Mizuno, Y. Fukazawa, Y. Ishikawa, N. Kawabata, Nuclear Instruments and Methods in Physics Research Section A 515 (2003) 671.
[9] T. Ikagawa, J. Kataoka, Y. Yatsu, T. Saito, Y. Kuramoto, N. Kawai, M. Kokubun, T. Kamae, Y. Ishikawa, N. Kawabata, Nuclear Instruments and Methods in Physics Research Section A 538 (2005) 640.
[10] R. Sato, J. Kataoka, Y. Kanai, Y. Ishikawa, N. Kawabata, T. Ikagawa, T. Saito, Y. Kuramoto, N. Kawai, Nuclear Instruments and Methods in Physics Research Section A 556 (2006) 535.
[11] J. Kataoka, T. Toizumi, T. Nakamori, Y. Yatsu, Y. Tsubuku, Y. Kuramoto, T. Enomoto, R. Usui, N. Kawai, H. Ashida, K. Omagari, K. Fujihashi, S. Inagawa, Y. Miura, Y. Konda, N. Miyashita, S. Matsunaga, Y. Ishikawa, Y. Matsunaga, N. Kawabata, Journal of Geophysical Research A 115 (2010) 05204.
[12] H. Ashida, et al., in: Proceedings of IAC, IAC-08.B4.6.A4, 2008.
[13] M. Ohno, K.Goto, Y. Hanabata, H. Takahashi, Y. Fukazawa, M. Yoshino, T. Saito, T. Nakamori, J. Kataoka, M. Sasano, S. Torii, H. Uchiyama, K. Nakazawa, S. Watanabe, M. Kokubun, M. Ohta, T. Sato, T. Takahashi, H. Tajima, in: Proceedings of this issue, Nuclear Instruments and Methods in Physics Research Section A, submitted for publication.
[14] D. Bédérède, E. Bougamont, Ph. Bourgeois, F.X. Gentit, Y. Piret, G. Tauzin, Nuclear Instruments and Methods in Physics Research Section A 518 (2004) 15.
[15] J.E. Grove, GLAST LAT Technical Note, LAT-TD-01476-01, 2003 〈http://heseweb.nrl.navy.mil/glast/CM/rpt/DiodeswithShinetsuReportLAT-TD-01476-01.pdf〉.
[16] J. Kataoka, T. Saito, M. Yoshino, H. Mizoma, T. Nakamori, Y. Yatsu, Y. Ishikawa, Y. Matsunaga, H. Tajima, M. Kokubun, Journal of Instrumentation 7 (2012) P06001.
[17] Y. Hanabata, et al., Proceedings of SPIE 7732 (2010) 104.